

EPR and FMR of SiCN Ceramics and SiCN Magnetic Derivatives

Sushil K. Misra^{1,*} and Sergey I. Andronenko^{1,2}

¹ Department of Physics, Concordia University, Montreal, Canada, H3G 1M8

² Institute of Physics, Kazan Federal University, Kazan, Russian Federation, 420008

Abstract: Silicon nitro carbide, SiCN, exhibits excellent high-temperature properties. It can withstand temperatures of up to 1800° C, which is superior to those of Si, SiC and Si₃N₄. Magnetic composites, as well as electrically conductive ceramics on the basis of SiCN, can be developed. Therefore, SiCN constitutes a new class of materials for high-temperature electronics. SiCN ceramics, doped with the transition metal ions exhibiting superparamagnetic features are promising in building high-temperature magnetic and pressure sensors. EPR (electron paramagnetic resonance) and FMR (ferromagnetic resonance) techniques can provide important information on the properties of SiCN and its magnetic derivatives, in conjunction with structural, magnetic and electric measurements. In the present work, EPR signals due to *sp*²-hybridized carbon-related dangling bonds were recorded over the 4 - 300 K range. SiCN ceramics consist of nanoparticles of SiCN and a free carbon phase. The two EPR signals, which were only resolved at the higher frequencies of W (95 GHz) and G (170 GHz) bands are due to carbon-related dangling bonds present as (i) defects on the free-carbon phase and (ii) within the bulk of SiCN ceramic network. SiCN magnetic ceramics, doped with the Fe ions were synthesized at different pyrolysis temperatures in the range 600° - 1600°C. Several magnetic phases in SiCN/Fe composite are detected by EPR/FMR technique. The main sources of magnetism in these samples are: (i) superparamagnetic nanoparticles of Fe₃Si, (*T*_C = 800°C), (ii) nanoparticles of Fe₃Si₃ (*T*_C = 393°C), which appear above 1000°C in single-domain state and (iii) nanoparticles of Fe₇₀Si_xC_{30-x} (620°C).

Keywords: Antiferromagnetic interaction, Curie law, Curie temperature, Dangling bonds, EPR, EPR linewidth, Ferromagnetic nanoparticles, FMR, Fluctuations of the magnetization, High-frequency EPR, Multi-frequency EPR, Nanoparticles, Phase-transition, Silicon nitro carbide (SiCN) ceramics, SiCN/Fe ceramics, SiCN/Mn ceramics, Superparamagnetic nanoparticles, Superparamagnetism, Temperature dependence.

* Corresponding author Sushil K. Misra: Department of Physics, Concordia University, Montreal, Canada, H3G 1M8; Tel: +1 (514) 848-2424; Fax: +1 (514) 848-2828; E-mail: sushil.misra@concordia.ca

INTRODUCTION

Contemporary electronics widely uses silicon carbide MEMS (Micro- Electro-Mechanical Systems) technology (SiC-MEMS). SiC is a semiconductor with good mechanical and thermal stability, and a wide band-gap for stable electronic properties at elevated temperatures [1]. However, the processes associated with the fabrication of SiC-MEMS have been known to be time-consuming, costly and technically very challenging. A new class of polymer-derived ceramic, which essentially consists of Silicon Carbon Nitride (SiCN), was proposed recently. A starting material for SiCN synthesis is a liquid polymer, which can be easily shaped using micro-moulds or microphotolithography, and this is one of the advantages of SiCN. The commercial precursor CERASET™ (KiON group AG) (polyureasilazane) for the synthesis of SiCN ceramics is available. The liquid polymer is cross-linked at 400°C in nitrogen gas flow to create a solid transparent polymer, whose free-standing forms are then pyrolyzed, yielding a black-colored ceramic, which can withstand temperatures above 1800°C [2, 3]. This SiCN ceramic exhibits outstanding creep, hardness and oxidation resistance, which are superior to those of Si, SiC and Si₃N₄.

Electrically conductive SiCN polymer-derived ceramics were developed by Liew *et al.* [4], and its conductivity was further modified by boron-doping (SiBCN) or Al-doping (SiAlCN) [5]. It is, thus possible to produce complex isolator-conductive material structures and develop new MEMS-SiCN technique. The addition of polymers, containing different magnetic transition metal ions, to initial silazane precursor leads to the formation of superparamagnetic SiCN ceramics, which can be used as magnetic sensors [6]. SiCN ceramics possess excellent piezoelectric properties [7] and can be used in pressure sensors. The investigation of SiCN ceramics and its conductive and magnetic derivatives is of great interest for developing high-temperature sensor applications [8, 9]. Formation of the free-carbon phase, which influences physical properties, was investigated in polymer-derived SiCN ceramics in detail [10 - 14].

Li *et al.* [15] exploited FTIR, Raman and XRD techniques for the investigation of SiCN ceramics obtained by pyrolysis from CERASET™ precursor. It was observed that the free C phase is formed owing to fast heating upon pyrolysis. Latest molecular dynamics simulations show that aromatic bonded carbon (C) ions are described by graphene network structure in the SiCN ceramics [16]. The existence of free C in SiCN structure and its ordering affect both mechanical and electrical features of polymer-derived SiCN ceramics, remarkably.

The EPR investigations on SiCN and SiBCN ceramics derived from non-commercial polymer precursors were reported [11 - 13, 17]. The origin of the

EPR line observed in *a*-C:H, turbostratic carbon, multiwall carbon nanotubes and irradiated multiwall carbon nanotubes, possibly related to the free C phase, was also studied [18 - 20]. Multifrequency EPR technique was applied at 9.6, 95 and 170 GHz to study SiCN ceramics at different temperatures from 4 K up to 300 K [21]. The intense EPR line was observed in this ceramics, which are ascribed to carbon-related sp^2 -dangling bonds [21]. Latest verification of such identification of this EPR signal was obtained [22, 23]. The EPR signal in UV-irradiated SiCN films was associated with nitrogen-related dangling bonds [24]. The EPR signals in SiCN films were ascribed to sp^2 -carbon-related dangling bonds, threefold-coordinated Si dangling bonds and the trapped holes at Si atom, as it was found by Savchenko *et al.* [25].

It is possible to tailor the magnetic properties of polymer-derived SiCN/Fe composites from paramagnetic to superparamagnetic, and then to ferromagnetic, with a variation of synthesis conditions, pyrolysis temperature, silazane precursor and Fe-containing precursor. Superparamagnetic features of SiCN/Fe and SiCN/Mn ceramics could be used to construct spintronic devices [26, 27], exploited at extremely high temperatures. Magnetic Fe-doped SiCN ceramics (SiCN/Fe) can be synthesized by adding different Fe-containing compounds to the initial polymer precursor. The SiCN ceramics synthesized at $T > 1000^\circ\text{C}$ possess good thermal/mechanical features for high-temperature and high-pressure applications. SiCN ceramics doped with Mn (SiCN/Mn) can also be synthesized by adding different Mn-containing polymers to the initial precursor. Such SiCN ceramic composites are very promising for MEMS applications. Therefore, SiCN ceramics have been extensively investigated in the past few years [2 - 25, 28 - 30]. They are composed of nanoparticles having the mean size of 1.3 nm [11, 12, 28]. The crystallization and formation of such SiCN nanoparticles started above 1300°C as found by small angle X-ray scattering (SAXS) [11]. The existence of carbon nanoparticles was verified by the intensity ratio of D and G bands in Raman spectra for the samples pyrolyzed at 1000°C [13]. The size of carbon nanoparticles is also about 1 nm [11, 13]. The nanostructure of SiCN ceramics, consisting of free C phase and SiCN ceramic network, plays a very significant role in the magnetization of SiCN/Fe materials, as considered below. The free C phase can be organized in the so-called “cage” structure, as it was suggested for SiCO ceramics [29, 30]. The SiCN/Fe nanocrystalline structure is composed of different nanoparticles of various sizes. The magnetic coupling of the Fe magnetic moments inside little nanoparticles than gives rise to the superparamagnetism. These Fe-containing nanocrystallites can exhibit ferromagnetic behavior if their size is large enough. Recently great attention was paid to the synthesis and the investigations of SiCN polymer derived ceramics doped with iron-containing compounds [6, 31 - 49]. Saha *et al.* [31] firstly obtained polymer-derived magnetic SiCN/Fe ceramic composites from CERASET™ solution using Fe_2O_3

powder. SiCN ceramics with the addition of ferrocene were synthesized by Dimitru *et al.* [32, 33]. The superparamagnetic behavior of SiCN/Fe magnetic ceramics was also observed by Li *et al.* [34, 35]. SiCN/Fe ceramics was investigated by FMR/EPR, IR and Raman spectroscopy, XRD and by measurements of magnetic features by Andronenko *et al.* [49]. FMR/EPR spectroscopy was utilized successfully to separate various types of magnetisms in SiCN/Fe ceramics, revealing at least three of them:

- i. ferromagnetic nanoparticles of $\text{Fe}_5\text{Si}_3\text{C}_x$,
- ii. ferromagnetic clusters distributed in the free C phase and, probably,
- iii. new Fe-containing nanocrystallites can appear at pyrolysis temperature above 1250°C and FMR/EPR spectra reflect such transformation.

Several kinds of Fe-containing crystallites, such as $\alpha\text{-Fe}$, Fe_3Si and Fe_5Si_3 were found in SiCN/Fe composites [46 - 48]. Recent investigations of magnetic properties of polymer-derived SiCN/Fe ceramics clearly show their predominantly superparamagnetic behavior with blocking temperature from 20 K [6] to 100 K [34, 35], the absence of coercive fields, remanent magnetization and rather wide distribution of nanoparticle sizes.

Yan *et al.* [37] found that Mn_5Si_3 nanocrystallites determine the magnetic properties of polymer-derived SiCN/Mn composite obtained by the addition of Mn metal powder to liquid CERASET™. This result agrees with the conclusion that $\text{Mn}_5\text{Si}_3\text{C}_x$ nanoparticles are the main source of magnetism in SiCN/Mn composites, synthesized by the use of manganese (II) acetylacetonate [50].

The EPR technique can be applied successfully to study magnetic SiCN ceramics activated with transition metal ions. It is the purpose of this review to summarize the results of EPR investigations of carbon-related dangling bonds in polymer-derived SiCN nanoceramics at several frequencies, as high as 170 GHz. Furthermore, this review will report the results of the EPR/FMR investigation on SiCN/Fe and SiCN/Mn ceramics obtained from liquid polyureasilazane precursor [21, 49, 50], to present detailed data on the origin of the various sources of magnetism contributed in these ceramics.

SYNTHESIS AND STRUCTURE

The fabrication procedure of SiCN ceramics is described elsewhere [2, 3]. Liquid polymer precursor CERASET™ (polyureasilazane) was crosslinked at 400°C for 60 min to fabricate transparent solid polymers. Thereafter, the crosslinked polymer was pyrolyzed at temperatures of 1000° , 1050° , 1100° , 1150° and 1200°C under nitrogen-gas flow to yield solid ceramic samples. The aim of pyrolysis was to exclude the C excess in the form of CH_4 molecules and to

precipitate free C, resulting in the incorporation of some amount of C ions into the mixed tetrahedra $\text{Si}(\text{C}_{1-x}\text{N}_x)_4$. The composition of SiCN ceramics pyrolyzed at 1100°C was determined to be $\text{SiC}_{0.74}\text{N}_{0.67}$; 30 wt % of C was in the free C phase as derived by elementary chemical analysis and relative intensity of NMR signals from the free-C and bound C ions.

SiCN/Fe Ceramics

The samples of magnetic SiCN/Fe ceramics were prepared by utilizing liquid polyureasilazane (CERASET™) precursor [49], to which 5-10 wt % of Fe (III) acetylacetonate was added. To fabricate a transparent dark-red solid polymer, the samples were cross-linked at 400°C for 90 min. Thereafter, the cross-linked polymer was pyrolyzed at $T = 600^\circ\text{C}$ - 1600°C in N gas flow. The composition of polymer-derived ceramics, as derived from elementary chemical analysis, was determined to be $\text{SiC}_{0.68}\text{N}_{0.41}$ at pyrolysis temperatures of 1100°C . The content of N decreased to 0.15 at high pyrolysis temperatures, accompanied by 30 wt % of C in the free C phase. The amount of Fe content determined by neutron-activated analysis of SiCN/Fe composite was to be of 0.2 wt %. The X-ray powder patterns for SiCN samples synthesized in this way at various pyrolysis temperatures were discussed by Andronenko *et al.* [49]. These X-ray patterns were similar to those, obtained for pure SiCN ceramics [51, 52] synthesized at 1450°C . The presence of peaks due to Fe_5Si_3 particles having a hexagonal structure was revealed in high-resolution X-ray patterns [53]. A weak peak owing to α -Fe particles was also detected.

SiCN/Mn Ceramics

The samples of magnetic SiCN/Mn ceramics were prepared [50], using liquid polyureasilazane (CERASET™) precursor, with an addition of 1 wt % of Mn (II) acetylacetonate $\text{Mn}(\text{C}_5\text{H}_7\text{O}_2)_2$. The thermal treatment was fulfilled in the same way as for SiCN/Fe ceramics [50].

PURE SiCN: EPR OF CARBON RELATED DANGLING BONDS

A Bruker X-band (9.6 GHz) EPR spectrometer (ER-200D) equipped with oxford helium gas-flow temperature controller at Concordia University was utilized to measure the EPR spectra in the different SiCN ceramics in the temperature interval from 4 K to 300 K [21]. The EPR spectra measured at $T = 295\text{ K}$ in SiCN samples, pyrolyzed at different temperatures, are shown in Fig. (1).

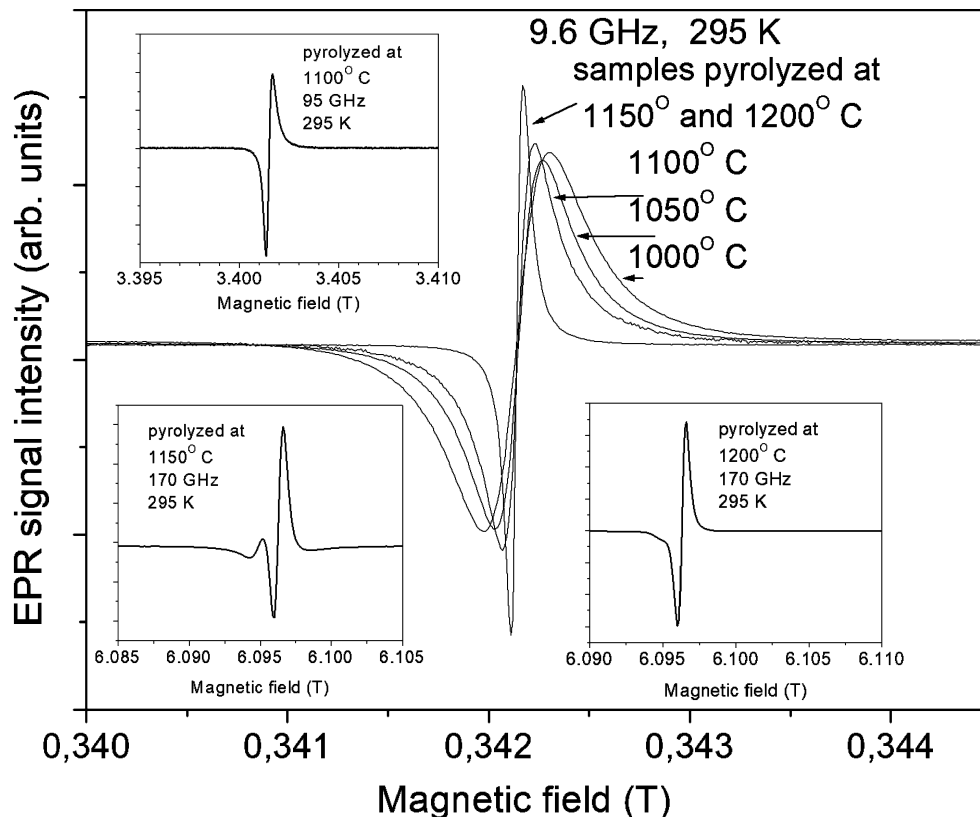


Fig. (1). EPR spectra of C-related dangling bonds in the different SiCN ceramics at 295 K. The inset shows W-band (95 GHz) EPR spectrum at 295 K. Reused from [21] with the Permission from AIP Publishing LLC.

Room-temperature EPR studies of pure SiCN samples were also performed at W-band (95 GHz) and G-band (170 GHz) at Cornell University. Only one intense EPR signal at $g = 2.0027 \pm 0.0001$ was detected at room temperature at X-band for all investigated samples. The g -value was measured using 2,2-Diphenyl-1-picrylhydrazyl (DDPH) as a reference sample. NMR Bruker gaussmeter was used for the magnetic field calibration for all investigated SiCN samples. The obtained g -value proved unambiguously that the observed EPR line in the investigated samples is caused by C-related defects [54, 55], rather than that from the Si dangling bonds ($g = 2.005$) [55].

The exchange narrowing of EPR linewidth (0.07 mT) was found for pure SiCN samples synthesized at 1150°C and 1200°C at X-band frequencies and was

explained by the increase of the spin concentration of dangling bonds emerged in the free C phase. Moreover, the spin concentration of the carbon dangling bonds is unchanged in the samples as there is no oxidation process and the H atoms are completely removed (above 1150°C), as confirmed by chemical analysis. This narrow EPR signal can be utilized as a *g*-marker at X-band. The dependences of the X-band EPR linewidth and wt % of H content versus pyrolysis temperature are represented in Fig. (2).

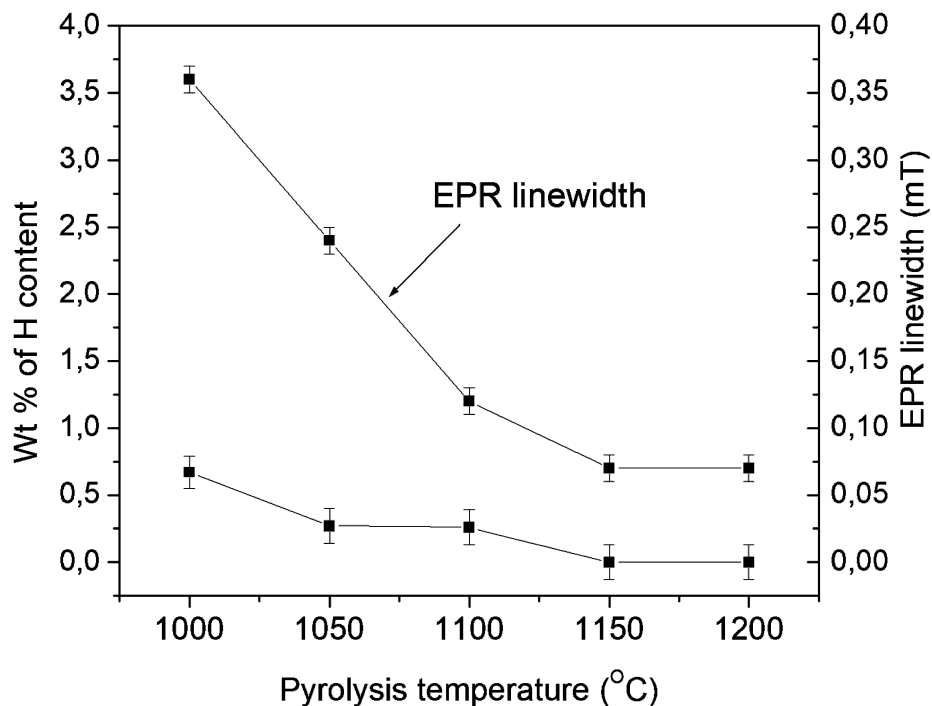


Fig. (2). The plot of the EPR linewidth and hydrogen content depending on the pyrolysis temperature of the samples. Reused from [21] with the Permission from AIP Publishing LLC.

The 95-GHz, W-band and EPR spectrum at 295 K agreed with that recorded at X-band, whereas the G-band (170 GHz) room-temperature spectrum showed the existence of second, less intense signal with larger *g*-factor, which can be associated with the shoulder revealed in X-band spectra at 4 K. The EPR spectra in the temperature interval of 4-295 K for the SiCN ceramics have mostly Lorentzian lineshape. The visible deviation from Lorentzian lineshape at X-band found for the samples pyrolyzed at 1150°C and 1200°C, can be interpreted by the

overlapping of two EPR signals, which were distinguished at G-band. This takes place when a minimum of one signal overlaps with the maximum of the other signal. Total EPR lineshape of these two overlapping signals turned out to be similar to Dysonian lineshape [56] at X- and W-bands.

A “shoulder” on the EPR line recorded at 4 K on the sample of SiCN pyrolyzed at 1150° C was observed and assigned to another EPR line, also related to carbon-related dangling bonds with $g = 2.0032$. They both decreased with a rise of the pyrolysis temperature, assuming that the amount of dangling bonds enhances with removing more H ions. The increase in the spin concentration of the dangling bonds results in the formation of the clusters and finally in exchange narrowing of the EPR line. The spin concentration of the dangling bonds was evaluated by comparison of the EPR signal integral intensity with that of a “strong-pitch” standard sample with known spin concentrations at X-band frequencies. The average number of spins was found to be of 10^{18} per cm^3 in all SiCN samples.

The EPR lineshape was revealed to be almost symmetrical for the samples pyrolyzed at $T < 1100^\circ\text{C}$. The linewidth at W-band for the sample synthesized at 1100° C is 0.32 mT at 295 K, which is twice larger than observed at X-band (= 0.14 mT). For the samples synthesized at 1150° C and 1200° C, two EPR signals were resolved at G-band with $g = 2.0027 \pm 0.0001$ and $g = 2.0032 \pm 0.0002$ which have different intensity and linewidth. The enhancement in the linewidth at higher frequencies can be explained by g -strain broadening, which becomes apparent with frequency increase.

The intense EPR signal at $g = 2.0027$ is caused by the dangling bonds that exist in the surface defects of the free C phase, while the less intense EPR signal with slightly higher g -factor (2.0032) is from the carbon-related dangling bonds that exist in the Si-C-N tetrahedra. The temperature-independent $g = 2.0027$ is similar to the g -value observed for glassy graphite samples caused by the high density of localized states at the Fermi level [18]. At the same time, it is far from the EPR signals at $g = 2.018$, 2.02 and 2.012, which were observed in planar graphite phase [18], turbostratic carbon [19] and multiwall carbon nanotube phase [20], correspondingly, and have ordered networks. Therefore, it was assumed that the SiCN ceramics under investigation do not contain ordered C networks. Alternatively, the EPR line with $g = 2.0032$ can be assigned to sp^3 -carbon related dangling bonds, associated with bulk “free” carbon phase.

Temperature Variation of the EPR Linewidth and Estimation of Exchange Interaction

The EPR linewidth has strong temperature dependence as represented in Fig. (3) for X-band. The temperature dependence of the EPR linewidth in the liquid-

helium temperature range was well described by the exchange interactions in amorphous materials between carbon dangling bonds as deduced by Misra [57]. Accordingly,

$$\Delta B = A' + B'*T + C'/(1 + \exp(J/T)). \quad (1)$$

In this expression, A' , B' , C' are constants and T is the temperature. The second term describes the linewidth broadening due to exchange coupling between spins modulated by vibrations via the spin-orbit coupling of the spins. This linear contribution (B') is negligible for the EPR linewidth in pure SiCN. The third term here, represents the contribution to the linewidth due to cross-relaxation wherein, an electron spin relaxes by simultaneous transitions between its energy levels and that of an exchange-coupled pair.

The value of antiferromagnetic interaction (J) was rather large, as it was found by fitting to EPR linewidth data, being anywhere from -12.5 to -15.1 K, as listed in Table 1, which also contains the values of the parameters A' , B' and C' .

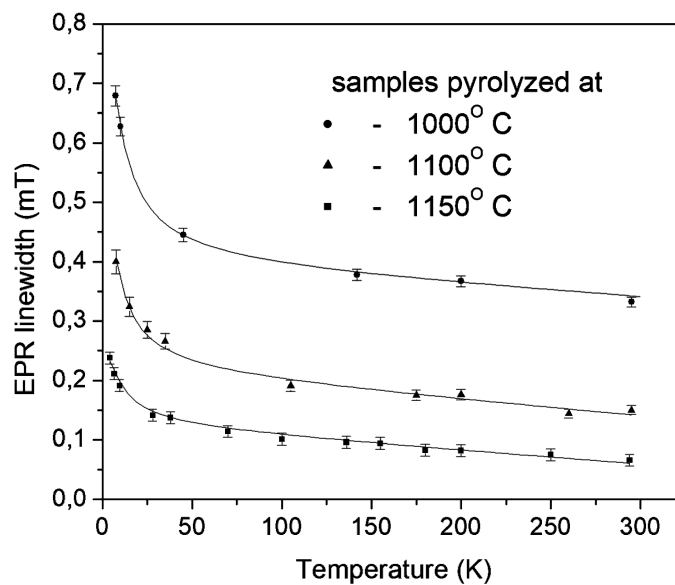


Fig. (3). Temperature variation of the EPR linewidth in the different SiCN ceramic samples. The circles, solid squares and triangles designate experimental data; the lines are fitting to eq. (1) using the parameters listed in the Table 1. Reused from [21] with the Permission from AIP Publishing LLC.

Table 1. Parameter fitting to eq. (1). Reused from [21] with the Permission from AIP Publishing LLC.

Pyrolysis temperature	A' (mT)	B' (mT/K)	C' (mT)	J (K)
1000° C	0.02±0.01	-0.0002±0.0002	0.74±0.05	-15.1±0.05
1100° C	-0.06±0.02	-0.0002±0.0002	0.55±0.05	-13.2±0.05
1150° C	-0.01±0.01	-0.0002±0.0002	0.27±0.05	-12.5±0.05

EPR STUDY OF SiCN/Fe AND THE TRANSFORMATIONS AT VARIOUS PYROLYSIS TEMPERATURES

EPR/FMR Spectra of SiCN/Fe Ceramics

An X-band (~9.5 GHz) Bruker ER-200D SRC EPR spectrometer equipped with the nitrogen-flow Bruker variable temperature assembly was utilized to study the SiCN/Fe ceramic samples in the temperature range 77-350 K [49]. Fig. (4) represents room-temperature EPR spectra of the different samples synthesized at various temperatures.

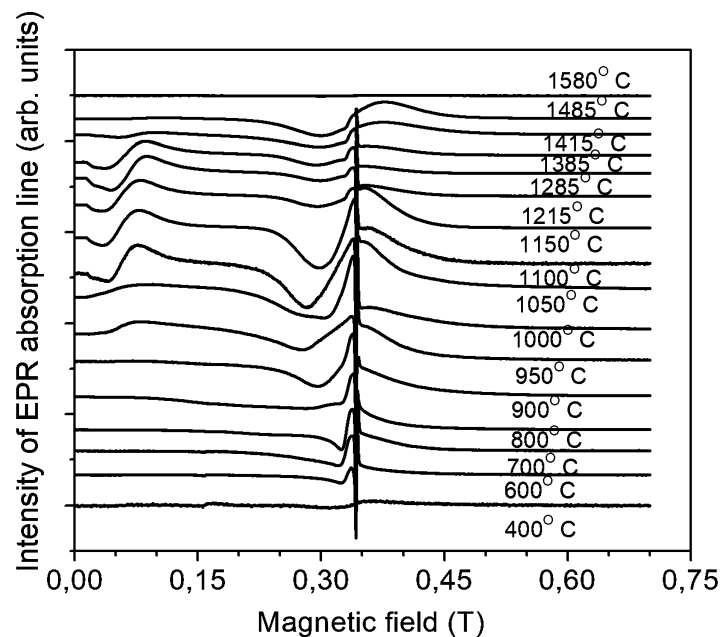


Fig. (4). The plot of Fe FMR/EPR spectra depending on the pyrolysis temperature of the SiCN/Fe samples measured at 295 K. Reproduced from [49] with the Permission from Springer.

The FMR signals, belonging to Fe-containing ferromagnetic crystalline particles, were observed in SiCN/Fe composites. Similarly to SiCN ceramics, narrow EPR line due to dangling bonds was also observed. Numerous transformations of SiCN/Fe ceramics were found from the temperature behavior of these EPR/FMR lines, namely, the dependencies of the linewidth and double-integrated intensity of the first-derivative EPR/FMR signals on the pyrolysis temperature. The explanation of the different EPR/FMR lines can be presented as follows.

(a) Narrow EPR signal caused by dangling bonds with $g = 2.0027$. The double-integrated intensity (per 1 mg) of the first-derivative line owing to sp^2 carbon dangling bonds with g -value of 2.0027 is presented in Fig. (5a). Fig. (5b) shows the dependence of the EPR linewidth on the pyrolysis temperature for the different samples.

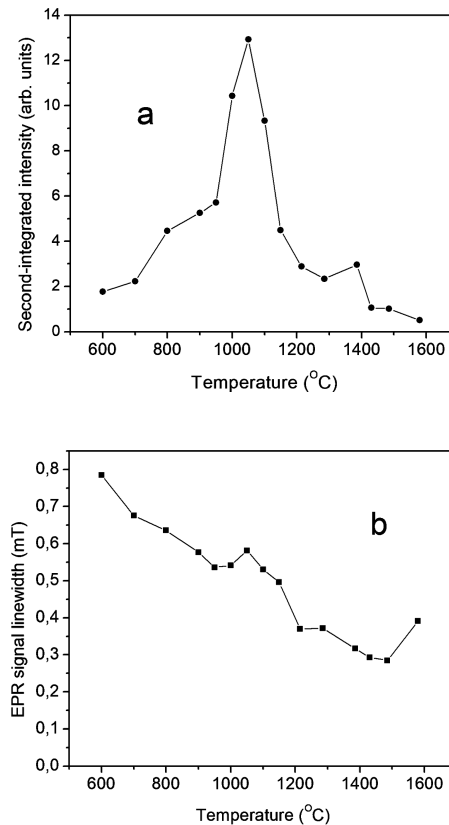


Fig. (5). Dependence of the double-integrated intensity (a) and EPR linewidth (b) of the first-derivative EPR line from dangling bonds on pyrolysis temperature measured in the different SiCN/Fe samples. Reproduced from [49] with the Permission from Springer.

The peak-to-peak width of EPR line from dangling bonds in SiCN/Fe samples pyrolyzed at 1100°C, was found to be larger (0.24 mT and 0.53 mT for 1 and 10 wt. % iron acetylacetonate, respectively) than that in the pure SiCN samples (0.12 mT), pyrolyzed at 1100°C. The dipole-dipole couplings between carbon dangling bonds and Fe³⁺ ions can be the reason of the linewidth increase.

(b) Fe³⁺ related EPR signal at $g \sim 2.0$. The dependence of the double integral of the first-derivative EPR signal (per 1 mg), on the pyrolysis temperature is shown in Fig. (6). The peak-to-peak linewidth of the first-derivative EPR signal as a function of the pyrolysis temperature is presented in Fig. (7).

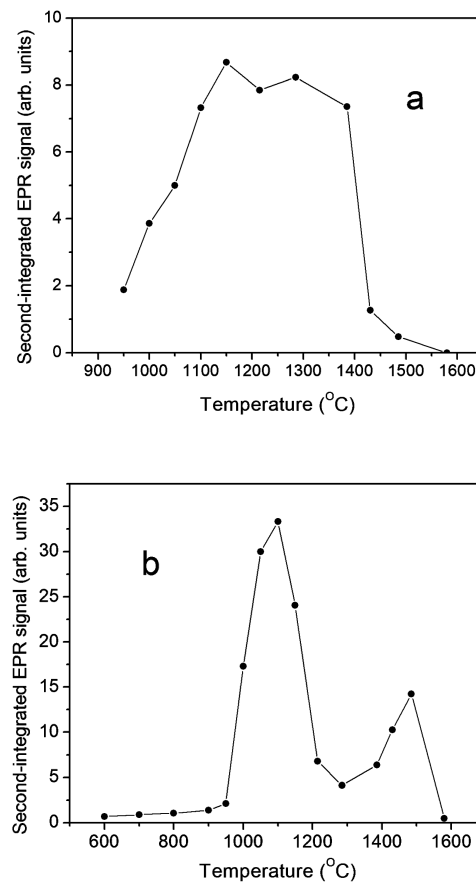


Fig. (6). The plot of the double-integrated intensity of Fe FMR/EPR line depending on pyrolysis temperature of the SiCN/Fe samples: a) for the signal with $g \sim 10$; b) for the broad signal with $g \sim 2.0$. Reproduced from [49] with the Permission from Springer.

It has been shown in Fig. (4) that this line composes of two overlapped broad signals (B1 and B2) with different linewidths for the samples pyrolyzed in the temperature range of 950°C- 150°C.

The linewidth of the EPR signal B1 varies considerably with temperature. The maximum width for EPR signal B1 was observed for the SiCN/Fe sample pyrolyzed at 1000°C (Fig. 7a). Whereas, the only linewidth of the B2 signal slightly increases (see Fig. 7b).

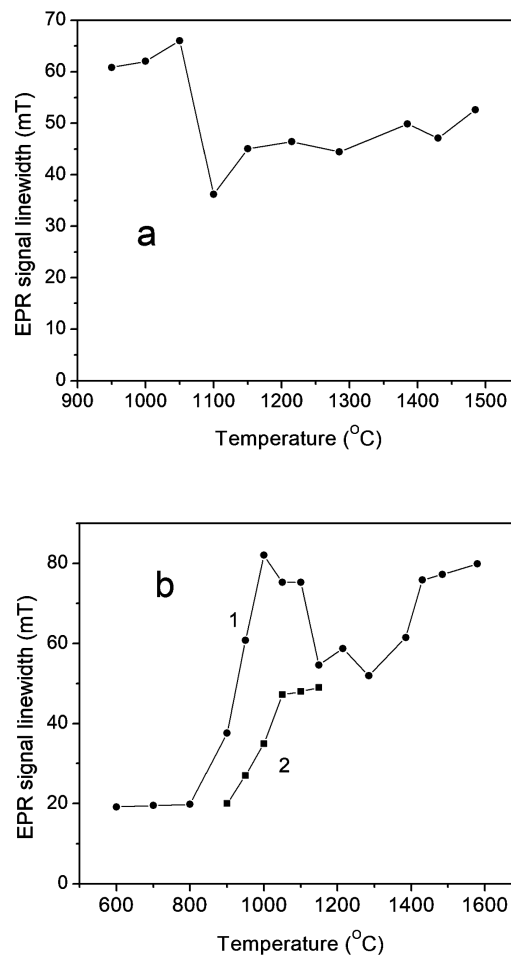


Fig. (7). The plot representing the Fe FMR/EPR linewidth at room temperature depending on the pyrolysis temperature of the SiCN/Fe samples: a) for the signal with $g \sim 10$; b) for the broad signal with $g \sim 2.0$ (filled circles and filled squares indicate the two coincided lines). Reproduced from [49] with the Permission from Springer.

The shape of line B1 corresponds to the EPR line of the assembly of superparamagnetic particles diluted in the diamagnetic matrix, as shown by Kliava *et al.* [58].

A correlation between the double-integrated intensity of the EPR signal of dangling bonds depending on the pyrolysis temperature, and the double-integrated intensity of the FMR signal that occurs at $g \sim 2.0$ was observed, as shown in Figs. **(5a and 6b)**.

As the double-integrated intensity of EPR signal related to dangling bonds is proportionate to the amount of free C phase in SiCN ceramics, we could suppose, that these magnetically ordered Fe ions are incorporated into the free-carbon phase. The characteristics of the EPR lines from the different SiCN/Fe samples synthesized at various temperatures can be described as follows.

(i) The Fe ions are in the paramagnetic state in the SiCN samples synthesized at temperatures 600°C-800°C, when SiCN samples are still “preceramized”. Their magnetization is rather small, as confirmed by the low magnitude of the double-integrated intensity of EPR signal.

(ii) The double-integrated intensity of the first-derivative Fe-related line increases for the SiCN/Fe samples synthesized at $T = 800^\circ\text{C}$ -1150°C, though the total Fe content is unchanged. This assumes that the increase of the Fe magnetic moment is caused by the formation of magnetically ordered Fe-containing nanocrystallites.

(iii) The double-integrated intensity of the wide signal at $g \sim 2.0$ reduced for the SiCN/Fe samples pyrolyzed above 1150°C. However, a third narrow Fe signal, centered at $g \sim 2$, appeared in this sample, assuming that a part of the Fe ions transfers to a new magnetic structural state.

(iv) The double-integrated intensity of the broad EPR signal at $g \sim 2.0$ increased again for the SiCN/Fe samples pyrolyzed at $T = 1400^\circ\text{C}$ -1500°C as it follows from Fig. **(6b)**. The reason is that EPR signal with $g \sim 10$ vanishes at these temperatures and the Fe ions, preliminarily incorporated in the Fe_5Si_3 crystallites, start to contribute to the EPR signal at $g \sim 2.0$.

(c) The EPR signal at $g \sim 10.0$. This signal is caused by the formation of ferromagnetic crystallites, which arise in the SiCN ceramics at the pyrolysis temperature of 950°C. It totally vanished for the samples pyrolyzed at 1430°C and above. These magnetic crystallites reveal ferromagnetism rather than superparamagnetism, for which a smaller size of the particle by order of SiCN ceramics grain (1.3 nm), is necessary. As shown below, it is probable that these ferromagnetic crystallites are Fe_5Si_3 nanoparticles, which follow from its low

value of Curie temperature ($T_C = 393$ K) [59]. Note that the Curie temperature of Fe_3Si , the other possible nanocrystallite, is much higher, $T_C = 800$ K [60], therefore, probably only the EPR line near $g = 2.0$ can be related to such kinds of compounds.

(d) The weak EPR signal at $g \sim 2.0$. This line emerges only in SiCN/Fe samples pyrolyzed at $T > 1215^\circ\text{C}$ when the crystallization of SiCN network takes place. The linewidth of this signal is rather narrow, being about 10 mT. It vanishes totally in the samples pyrolyzed at $T > 1485^\circ\text{C}$. It can be assigned to the Fe^{3+} ions incorporated in Si_3N_4 nanocrystallites, which begin to crystallize at 1200°C , as revealed by XRD analysis.

(e) The samples pyrolyzed above 1500°C . No EPR signals from the Fe^{3+} ions were observed in these samples, owing to the evaporation of Fe ions from SiCN ceramics at $T > 1530^\circ\text{C}$, corresponding to the iron melting temperature.

Temperature Dependence of Fe^{3+} EPR Lines

(i) The EPR line at $g \sim 10$. The double-integrated intensity (per 1 mg) of the first-derivative EPR line and the peak-to-peak width of the EPR line from the SiCN ceramic sample pyrolyzed at 1100°C in the temperature interval 77 - 350 K are shown in Figs. (8a and 8b), correspondingly. As it follows from Fig. (8a), the double-integrated intensity of this signal vanished at about 380 ± 10 K. The behavior of EPR linewidth is also consistent with the temperature variation of the magnetic moment of the ferromagnetic Fe_5Si_3 particles with the Curie temperature of 393 K. It can be proved by fitting with the following formula obtained for the temperature (T) variation of the FMR linewidth of impurity centers in ferromagnetic sample [61]:

$$\Delta B = \Delta B_0 + P|T_c - T|^{-0.7} \quad (2)$$

The fit to eq. (1) gave the following values $\Delta B_0 = (22.0 \pm 1.0)$ mT, $P = (0.52 \pm 0.05) \times 10^3 \text{ K}^{0.7} \times \text{mT}$, and $T_C = (393 \pm 5)$ K. The Curie temperature, obtained from this fitting, is the same as $T_C = 393$ K determined for Fe_5Si_3 [59].

The linewidth expression described by eq. (2) is explained as follows. A significant contribution to FMR linewidth in ferromagnetic samples is caused by the magnetization fluctuations M close to the Curie temperature.

As the magnetization shifts the resonance position, magnetization fluctuations cause the resonance signal broadening. Thus, following the theory of second order phase transition [62] and applying the scaling theory [63], the mean-square

magnetization fluctuations can be expressed as:

$$\langle (\Delta M)^2 \rangle = \frac{T_c \chi}{V} \propto |T_c - T|^{-1.4} \quad (3)$$

here, χ is magnetic susceptibility, V is volume and T_c is Curie temperature.

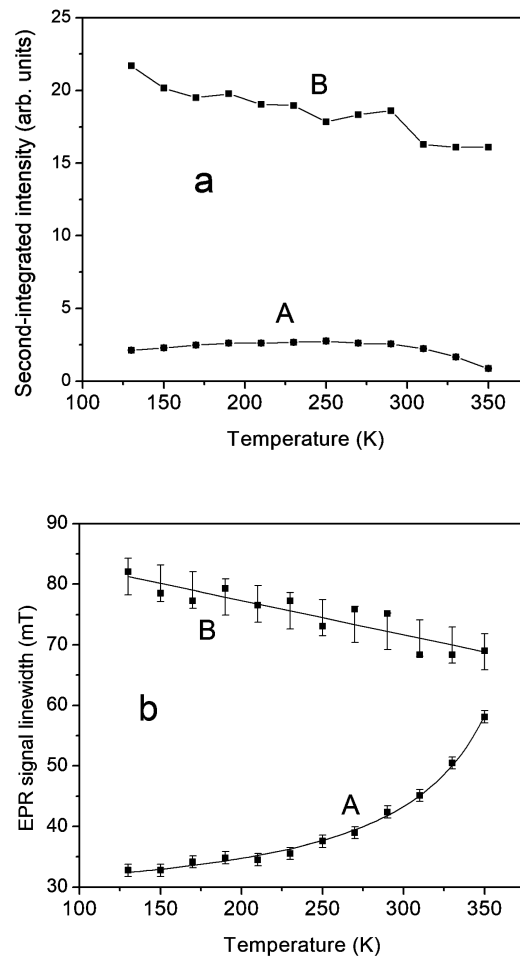


Fig. (8). Temperature variation of the double-integrated intensity (a) and the FMR/EPR linewidth of the first-derivative FMR/EPR line (b) (Reproduced from [49] with the Permission from Springer): a) for the signal at $g \sim 10.$; b) for the signal at $g \sim 2.0.$ The solid lines correspond to the fitting results with the parameters reported in the text.

Hence, the fluctuation M is inversely proportionate to the square root of the temperature deviation from the Curie point (T_c) [62]. The EPR linewidth, ΔB , is proportionate to the mean square of magnetization fluctuations M resulting in eq. (2).

(ii) The intense EPR line at $g=2.065\pm 0.001$. This signal does not reveal considerable temperature dependence. Its linewidth can be described by the linear expression: $\Delta B(T) = \Delta B_0 + PI \cdot T$, where $\Delta B = (89.0 \pm 2.0)$ mT and $PI = (-0.056 \pm 0.008)$ mT/deg. It is supposed here that the Fe ions are in the superparamagnetic state, confirmed by the following facts.

- (a) The g -factor is 2.065.
- (b) The temperature variation of double-integrated intensity follows, within the range of measurement error, the Curie law in this temperature range of 77-350 K.
- (c) The double-integrated intensity, being proportional to its magnetic moment, rises significantly with the enhancement of the pyrolysis temperature of the SiCN/Fe samples ($T > 1000^\circ\text{C}$).
- (d) The Fe ions content in the SiCN/Fe samples remain unchanged; therefore, this increase in the double-integrated intensity can only be caused by the formation of the magnetically ordered Fe-containing nanocrystallites.

The investigation of the bulk magnetization of SiCN/Fe ceramics using a vibration sample magnetometer is very helpful along with the study of collective magnetic moments using the EPR/FMR method. The magnetization versus the magnetic field of some SiCN ceramic samples was studied at 295 K in a magnetic field of up to 2.2 T. Almost no hysteresis or remanent magnetization was found in the investigated samples [49]. The coercive field decreases for the SiCN/Fe samples synthesized at 700°C from about 15 mT to zero for the samples synthesized at 1200°C - 1500°C . The SiCN/Fe samples definitely exhibit superparamagnetic behavior. Large coercive fields for SiCN/Fe samples prepared at 700°C can be due to ferromagnetic α -Fe particles. The temperature variation of the magnetization at the magnetic field of 0.1 T was studied in the interval of 150 - 700 K as represented in Fig. (9).

It was clearly observed from this dependence that there were two various contributions to the magnetization of SiCN/Fe sample synthesized at 1215°C : the ferromagnetic contribution having the phase-transition temperature of $T_c = 390$ K, and the superparamagnetic contribution, obeying the Curie law.

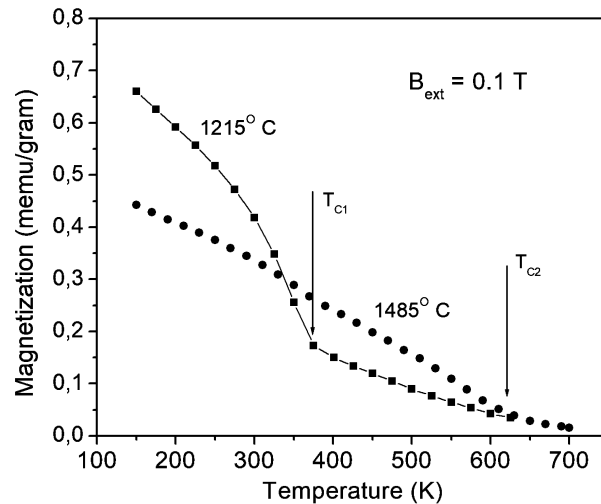


Fig. (9). Temperature variation of the magnetization measured in SiCN/Fe samples prepared at various temperatures at 0.1 T. Reproduced from [49] with the Permission from Springer.

The obtained Curie temperature (390 K) is due to Fe_5Si_3 , as confirmed by the EPR/FMR experiments. The low-field FMR line was observed only in the SiCN/Fe sample pyrolyzed above 950°C , that corresponds well to Si-Fe phase diagram [64] for Fe_5Si_3 formation.

The magnetic transition at 620 K was revealed for the SiCN/Fe ceramics synthesized at 1485°C , which is related to a new ferromagnetic phase, most probably, $\text{Fe}_{70}\text{Si}_x\text{C}_{30-x}$ phase with $T_c = 620$ K [65]. No peculiarities in the dependence of magnetization on temperature near 490 K, the Curie temperature for Fe_3C nanoparticles, were observed [66]. It implies that no such Fe-containing particles were formed in SiCN/Fe. The variation of saturation magnetization with the pyrolysis temperature is analogous to that of the dependence of the double-integrated intensity of the low-field EPR signal. Hence, the main part of the magnetization in SiCN/Fe ceramics is caused by the nanoparticles of Fe-containing crystallites, very likely to those of Fe_5Si_3 .

EPR/FMR STUDY OF SICN/MN CERAMICS

An X-band EPR Bruker ER-200D SRC spectrometer equipped with nitrogen-flow Bruker variable temperature assembly was utilized to study the SiCN/Mn ceramic samples [50]. The SiCN/Mn samples pyrolyzed at 1100°C were investigated. The EPR/FMR signals measured at various temperatures from 77 to 350 K are

represented in Fig. (10).

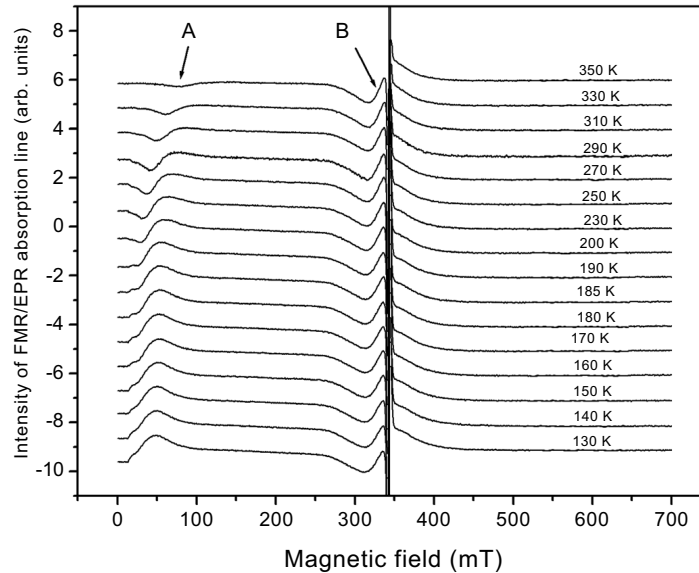


Fig. (10). Temperature dependence of the first-derivative signals. Here A and B designate the FMR and EPR lines, correspondingly. Reproduced from [50] with Permission from Springer.

FMR lines

The FMR signal (A) centered at ~ 65.0 mT with a linewidth of ~ 80.0 mT was observed in this SiCN/Mn sample at $T = 295$ K. The intensity of this signal rises with a decrease in temperature. It represents a structure on the low-field side with a decrease in temperature. This signal is caused by the ferromagnetic particles of the $Mn_5Si_3C_x$ distributed over the SiCN/Mn sample. Additionally, the EPR line (B) was observed, situated at ~ 340.0 mT with almost constant EPR linewidth (~ 35.0 mT), which is due to Fe-containing superparamagnetic nanoparticles. The variation of the double-integrated intensity of the absorption line (per 1 mg) and the peak-to-peak linewidth of the first-derivative EPR/FMR signal are presented in the temperature interval 77 - 350 K in Fig. (11a) and Fig. (11b), respectively.

Critical temperature as determined from the FMR line A. The area under this absorption line, which was obtained by double integration of the first-derivative absorption curve, decreased monotonically from 290 K to the highest temperature of observation (350 K) as seen from Fig. (11a). This integral intensity is proportionate to the magnetization of the ferromagnetic particles of $Mn_5Si_3C_x$ in SiCN/Mn. The FMR linewidth of signal A was described by Eq. (2) [61] exhibiting the temperature (T) dependence. The fit yields the values: $\Delta B_0 = (23.0 \pm 1.0)$ mT, $P = (0.26 \pm 0.03) \times 10^3 \text{ K}^{0.7} \times \text{mT}$, and $T_c = 363 \pm 2$ K. A significant

contribution to the FMR linewidth in ferromagnetic samples is caused by the magnetization fluctuations, M , close to the Curie temperature, as explained for the FMR line in SiCN/Fe. The behavior of the FMR line in SiCN/Mn agrees with the temperature variation of the magnetization of the ferromagnetic $\text{Mn}_5\text{Si}_3\text{C}_x$ particles. The Curie temperature of 360 K corresponds to this chemical composition, as derived from the Mn-Si-C phase diagram [67, 68].

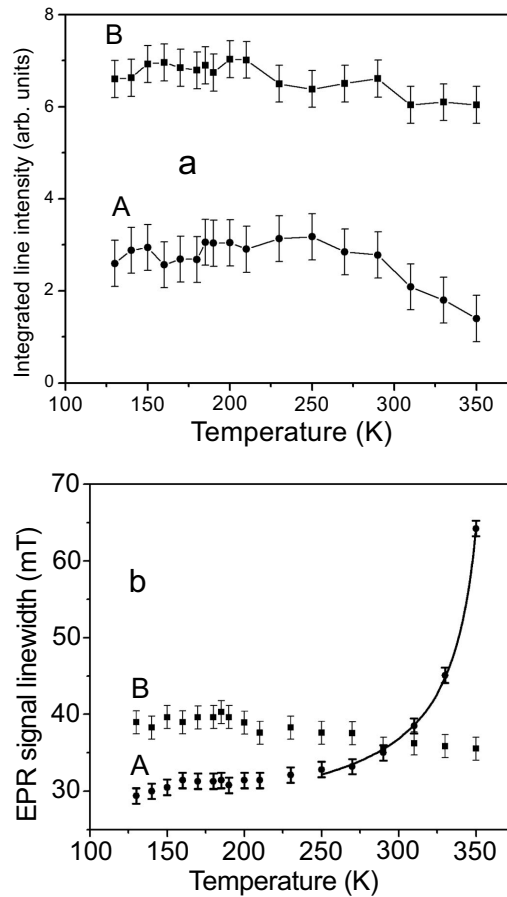


Fig. (11). Temperature dependence of the double-integrated intensity of first-derivative EPR/FMR line (a) and peak-to-peak first-derivative EPR/FMR linewidth (b) for the signals A and B. The solid line is fitting using the parameters, listed in the text. Reproduced from [50] with Permission from Springer.

EPR Lines

EPR lines were observed due to the two species as described below.

(i) *EPR signal from the dangling bonds.* The sharp, narrow signal with $g = 2.0026$ is caused by the carbon-related dangling bonds. Its EPR linewidth, e.g. 0.14 mT

for the sample with 1 wt % of $\text{Mn}(\text{C}_5\text{H}_7\text{O}_2)_2$ in the SiCN/Mn sample, was turned out to be slightly larger than those in the pure SiCN samples, *e.g.* 0.12 mT in pure SiCN samples synthesized at 1100°C [21]. The dipole-dipole couplings between C-related dangling bonds and the Mn^{2+} ions in the SiCN/Mn ceramics can be the reason for the additional contribution to the linewidth.

(ii) *The EPR signal owing to Mn superparamagnetic species (B).* This quite broad signal is centered at ~340.0 mT ($g = 2.05 \pm 0.01$). The position of this line and linewidth do not change in the temperature range 77 – 350 K. The EPR linewidth is ~ 35.0 mT. This EPR signal is caused by the superparamagnetic particles of the Mn-containing compound and it corresponds to the EPR line, calculated by Kliava *et al.* [58] for an assembly of superparamagnetic particles diluted in the diamagnetic matrix.

However, A and B lines correspond to different Mn-containing compounds, because their temperature dependencies are quite different from each other.

Only SiCN/Fe samples pyrolyzed at 1100°C were investigated here and therefore additional investigations are highly desirable for deeper understanding of magnetic transformations of SiCN/Mn ceramics depending on pyrolysis temperature.

CONCLUDING REMARKS AND DISCUSSION

A. Undoped SiCN. The most significant characteristics of the EPR spectra in undoped SiCN samples are as follows:

- (i) The two observed EPR signals are caused by C-related sp^2 -dangling bonds:
 - (a) more intense EPR signal at $g = 2.0027$ relates to the free C phase at the surface;
 - (b) less intense EPR signal at $g = 2.0032$ which was well resolved at 170 GHz relates to the bulk of SiCN ceramic network
- (ii) The EPR linewidth declines with a rise in pyrolysis temperature of a sample. This is due to exchange narrowing, which enhanced with the increase of a number of carbon-related dangling bonds. This number, in its turn, increases with the increasing pyrolysis temperature due to the removing of hydrogen ions.
- (iii) The EPR linewidth increases strongly with decreasing temperature in all samples. The antiferromagnetic interaction among dangling bonds in these samples as estimated from the temperature variation of the EPR linewidth is found to be rather strong, between –12 and –15 K.

(iv) The X-band EPR line, detected in pure SiCN samples pyrolyzed at 1150°C and 1200°C, is stable and very narrow. Therefore, they can be a prospective spin-probe at room temperature.

B. SiCN/Fe. The most important features of the SiCN/Fe samples are as follows.

(i) The SiCN/Fe ceramic samples, which consist of nanoparticles, pyrolyzed in the temperature range 600°C- 1580°C, were investigated by EPR/FMR.

(ii) Three different states of Fe³⁺ ions were revealed in SiCN/Fe samples:

(a) The ordered and amorphous free C phases exist in the SiCN/Fe samples, as well as the transformation from the paramagnetic to superparamagnetic state was observed in the sample pyrolyzed at temperatures 600°C-800°C and 950°C-1150°C, correspondingly.

(b) Fe₅Si₃ particles are characterized by ferromagnetic behavior. The EPR line corresponding to this phase emerges in the SiCN/Fe samples synthesized at 950°C and vanishes in the samples synthesized at 1400°C.

(c) The third type of Fe³⁺ ions exhibits the narrow signaling at $g \sim 2.0$, revealed only in the samples pyrolyzed at $T > 1200^\circ\text{C}$. They are possibly incorporated into the Si-C-N nanocrystallites. These lines vanish in the SiCN/Fe samples pyrolyzed at $T > 1530^\circ\text{C}$.

(iii). The techniques of EPR/FMR and magnetic measurements provide sufficient data on the characteristics of the SiCN/Fe nanoparticles and show that this material can be exploited for MEMS applications.

C. SiCN/Mn. The most significant features of the SiCN/Mn samples are as follows.

(i) The FMR and magnetization data show that SiCN/Mn samples exhibit ferromagnetic or superparamagnetic behavior and they do not show paramagnetic behavior, which is due to the individual Mn ions in spite of the rather small concentration of Mn (~0.2%).

(ii) Ferromagnetic particles of Mn₅Si₃C_x, or other composites, are formed upon pyrolysis. At the same time, superparamagnetic clusters can be formed if the particle size is less than 5 nm. The two various species of Mn ions are:

(a) nanoparticles associated probably with SiCN network, which manifests themselves by the broad EPR signal at $g \sim 2.0$. The magnetization of these particles is almost temperature-independent in the investigated temperature range;

(b) the nanoparticles, which relate to the formation of SiCN network (Mn-Si-N-C) mainly due to the formation of $Mn_5Si_3C_x$ nanoparticles, as derived here from the temperature variation of the low-field FMR line. These particles reveal a transition from ferromagnetic to paramagnetic phase at 363 K, corresponding to the $Mn_5Si_3C_x$ compound.

CONSENT FOR PUBLICATION

Not applicable.

CONFLICT OF INTEREST

The author (editor) declares no conflict of interest, financial or otherwise.



ACKNOWLEDGEMENTS

This research was supported by the Natural Sciences and Engineering Research Council of Canada (NSERC) (SKM); SIA is grateful to Ministry of Education of Russian Federation for partial support within the framework of research project (#3.2166.2017/4.6), allocated to Kazan Federal University.

REFERENCES

- [1] Wu, C.H.; Zorman, C.A.; Mehregany, M. Growth of polycrystalline SiC films on SiO₂ and Si₃N₄ on by APCVD. *Thin Solid Films*, **1999**, 355-356, 179-183. [http://dx.doi.org/10.1016/S0040-6090(99)00494-0]
- [2] Liew, L.-A.; Zhang, W.; Bright, V. M.; An, L.; Dunn, M. L.; Raj, R. *A*, **2001**, 89, 64-70.
- [3] Liew, L.-A.; Liu, Y.; Luo, R.; Cross, T.; An, L.; Bright, V.M.; Dunn, M. L.; Daily, J. W.; Raj, R. *A*, **2002**, 95, 120-134.
- [4] Liew, L.-A.; Saravanan, R.A.; Bright, V.M.; Dunn, M.L.; Daily, J.W.; Raj, R. Processing and characterization of silicon carbon-nitride ceramics: application of electrical properties toward MEMS thermal actuators. *Sensors and Actuators. A*, **2003**, 103, 171-181.
- [5] Hermann, A.M.; Wang, Y.T.; Ramakrishnan, P.A.; Balzar, D.; An, L.; Haluschka, C.; Riedel, R. Structure and electronic properties of Si-(B)- C-N ceramics. *J. Am. Ceram. Soc.*, **2001**, 84, 2260-2264. [http://dx.doi.org/10.1111/j.1151-2916.2001.tb00999.x]
- [6] MacLachlan, M.J.; Ginzburg, M.; Coombs, N.; Coyle, T.W.; Raju, N.P.; Greedan, J.E.; Ozin, G.A.; Manners, I. Shaped ceramics with tunable magnetic properties from metal-containing polymers. *Science*, **2000**, 287(5457), 1460-1463. [http://dx.doi.org/10.1126/science.287.5457.1460] [PMID: 10688788]
- [7] Zhang, L.; Wang, Y.; Wei, Y.; Xu, W.; Fang, D.; Zhai, L.; Lin, K.C.; An, L. A silicon carbonitride ceramic with anomalously high piezoresistivity. *J. Am. Ceram. Soc.*, **2008**, 91, 1346-1349. [http://dx.doi.org/10.1111/j.1551-2916.2008.02275.x]
- [8] Andronenko, S.; Stiharu, I.; Packirisamy, M.; Moustapha, H.; Dionne, P. The use of micro electromechanical systems for surge detection in gas turbine engines. *Proceedings of International Conference on MEMS, NANO, and Smart Systems*, Banff, Alberta, Canada July 24–27, 2005 Banff **2005**, pp. 355-358. [http://dx.doi.org/10.1109/ICMENS.2005.122]

- [9] Leo, A.; Andronenko, S.; Stiharu, I.; Bhat, R.B. Characterization of thick and thin film SiCN for pressure sensing at high temperatures. *Sensors (Basel)*, **2010**, *10*(2), 1338-1354. [http://dx.doi.org/10.3390/s100201338] [PMID: 22205871]
- [10] Saha, A.; Raj, R.; Williamson, D.V.; Kleebe, H-J. Characterization of nanodomains in polymer-derived SiCN ceramics employing multiple techniques. *J. Am. Ceram. Soc.*, **2005**, *88*, 232-234. [http://dx.doi.org/10.1111/j.1551-2916.2004.00034.x]
- [11] Trassl, S.; Motz, G.; Rossler, E.; Ziegler, G. Characterization of the Free-Carbon Phase in Precursor-Derived Si-C-N Ceramics: I, Spectroscopic Methods. *J. Am. Ceram. Soc.*, **2002**, *85*, 239-244. [http://dx.doi.org/10.1111/j.1551-2916.2002.tb00072.x]
- [12] Trassl, S.; Kleebe, H-J.; Stormer, H.; Motz, G.; Rossler, E.; Ziegler, G. Characterization of the Free Carbon Phase in Precursor-Derived SiCN Ceramics Part II: Comparison of Different Precursors. *J. Am. Ceram. Soc.*, **2002**, *85*, 1268-1274. [http://dx.doi.org/10.1111/j.1551-2916.2002.tb00256.x]
- [13] Trassl, S.; Motz, G.; Rossler, E.; Ziegler, G. Characterization of the free-carbon phase in precursor-derived SiCN ceramics. *J. Non-Cryst. Solids*, **2001**, *293-295*, 261-267. [http://dx.doi.org/10.1016/S0022-3093(01)00678-0]
- [14] Kleebe, H-J.; Störmer, H.; Trassl, S.; Ziegler, G. Thermal stability of SiCN ceramics studied by spectroscopy and electron microscopy. *Appl. Organomet. Chem.*, **2001**, *15*, 858-866. [http://dx.doi.org/10.1002/aoc.243]
- [15] Li, Y-L. Kroke, E.; Riedel, R.; Fasel, C.; Gervais, C.; Babonneau F. Thermal cross-linking and pyrolytic conversion of poly(ureamethylvinyl)silazanes to silicon-based ceramics. *Appl. Organomet. Chem.*, **2001**, *15*, 820-832. [http://dx.doi.org/10.1002/aoc.236]
- [16] Resta, N.; Kohler, C.; Treblin, H-R. Molecular dynamics simulations of amorphous Si-C-N ceramics: composition dependence of atomic structure. *J. Am. Ceram. Soc.*, **2003**, *86*, 1409-1414. [http://dx.doi.org/10.1111/j.1551-2916.2003.tb03484.x]
- [17] Berger, F.; Muller, A.; Albinger, F.; Muller, K. Solid state NMR investigation on Si-B-C-N ceramics derived from boron-modified poly(allylmethylsilazane). *Z. Anorg. Allg. Chem.*, **2005**, *631*, 355-363. [http://dx.doi.org/10.1002/zaac.200400259]
- [18] von Bardeleben, H.J.; Cantin, J.L.; Zeinert, A.; Racine, B.; Zellama, K.; Hai, P.N. Spins and microstructure of hydrogenated amorphous carbon: a multiple frequency electron paramagnetic resonance study. *Appl. Phys. Lett.*, **2001**, *78*, 2843-2845. [http://dx.doi.org/10.1063/1.1370980]
- [19] Coleman, J.N.; Dalton, A.B.; Curran, S.; Rubio, A.; Davey, A.P.; Drury, A.; McCarthy, B.; Lahr, B.; Ajayan, P.M.; Roth, S.; Barklie, R.C.; Blau, W.J. Phase separation of carbon nanotubes and turbostratic graphite using a functional organic polymer. *Adv. Mater.*, **2000**, *12*, 213-216. [http://dx.doi.org/10.1002/(SICI)1521-4095(200002)12:3<213::AID-ADMA213>3.0.CO;2-D]
- [20] Beuneu, F.; l'Huillier, C.; Salvétat, J-P.; Bonard, J-M.; Forro, L. Modification of multiwall carbon nanotubes by electron irradiation: An ESR study. *Phys. Rev.*, **1999**, *B59*, 5945-5949. [http://dx.doi.org/10.1103/PhysRevB.59.5945]
- [21] Andronenko, S. I.; Stiharu, I.; Misra, S.K. *Synthesis and characterization of polyureasilazane derived SiCN ceramics.*, **2006**, *99*, 113907 [http://dx.doi.org/10.1063/1.2202291]
- [22] Tomasella, E.; Spinelle, L.; Bousquet, A.; Rebib, F.; Dubois, M.; Eypert, C.; Gaston, J.P.; Cellier, J. Structural and Optical Investigations of Silicon Carbon Nitride Thin Films Deposited by Magnetron. *Plasma Process. Polym.*, **2009**, *6*, S11-S16. [http://dx.doi.org/10.1002/ppap.200930103]
- [23] Tomasella, E.; Rebib, F.; Dubois, M.; Cellier, J.; Jacquet, M. Structural and optical properties studies

- of sputtered a-SiCN thin films. *J. Phys. Conf. Ser.*, **2008**, *100*, 082045.
[<http://dx.doi.org/10.1088/1742-6596/100/8/082045>]
- [24] Kobayashi, K.; Yokoyama, H.; Endoh, M. Leakage current and paramagnetic defects in SiCN dielectrics for copper diffusion barriers. *Appl. Surf. Sci.*, **2008**, *254*, 6222-6225.
[<http://dx.doi.org/10.1016/j.apsusc.2008.02.144>]
- [25] Savchenko, D.; Kulikovskiy, V.; Vorliček, V.; Lanček, J.; Kiselov, V.; Kalabukhova, E. Optical and magnetic resonance study of a-SiC_xN_y films obtained by magnetron sputtering. *Phys. Status Solidi, B Basic Res.*, **2014**, *251*, 1178-1185.
[<http://dx.doi.org/10.1002/pssb.201451041>]
- [26] Fujimori, H.; Ohnuma, S.; Kobayashi, N.; Masumoto, T. Spintronics in metal-insulator nanogranular magnetic thin films. *J. Magn. Magn. Mater.*, **2006**, *304*, 32-35.
[<http://dx.doi.org/10.1016/j.jmmm.2006.02.005>]
- [27] Wolf, S.A.; Awschalom, D.D.; Buhrman, R.A.; Daughton, J.M.; von Molnár, S.; Roukes, M.L.; Chtchelkanova, A.Y.; Treger, D.M. Spintronics: a spin-based electronics vision for the future. *Science*, **2001**, *294*(5546), 1488-1495.
[<http://dx.doi.org/10.1126/science.1065389>] [PMID: 11711666]
- [28] Bill, J.; Kamphowe, T.W.; Muller, A.; Wichmann, T.; Zern, A.; Jalowieki, A.; Mayer, J.; Weinmann, M.; Schuhmacher, J.; Muller, K.; Peng, J.Q.; Seifert, H.J.; Aldinger, F. Precursor-derived Si-(B-)C-N Ceramics: Thermolysis, Amorphous State and Crystallization. *Appl. Organomet. Chem.*, **2001**, *15*, 777-793.
[<http://dx.doi.org/10.1002/aoc.242>]
- [29] Saha, A.; Raj, R.; Williamson, D.  model of the nanodomains in polymer-derived SiCO. *J. Am. Ceram. Soc.*, **2006**, *89*, 2188-2195.
- [30] Saha, A.; Raj, R. Crystallization map for SiCO amorphous ceramics. *J. Am. Ceram. Soc.*, **2007**, *90*, 578-583.
[<http://dx.doi.org/10.1111/j.1551-2916.2006.01423.x>]
- [31] Saha, A.; Shah, S.R.; Raj, R.; Russek, S.E. Polymer derived SiCN composite with magnetic properties. *J. Mater. Res.*, **2003**, *18*, 2549-2551.
[<http://dx.doi.org/10.1557/JMR.2003.0356>]
- [32] Dumitru, A.; Ciupina, V.; Stamatina, I.; Prodan, G.; Moroza, A.; Mirea, C. Plasma polymerization of ferrocene with silane and silazane monomers for design of nanostructured magnetic ceramics. *J. Optoelectron. Adv. Mater.*, **2006**, *8*, 50-54.
- [33] Dumitru, A.; Stamatina, I.; Moroza, A.; Mirea, C.; Ciupina, V. Si-C-N-Fe nanostructured ceramics from inorganic polymer precursors obtained by plasma polymerization. *Mater. Sci. Eng. C*, **2007**, *27*, 1331-1337.
[<http://dx.doi.org/10.1016/j.msec.2006.09.004>]
- [34] Li, Y.; Zheng, Z.; Reng, C.; Zhang, Z.; Gao, W.; Yang, S.; Xie, Z. Preparation of Si-C-N-Fe magnetic ceramics from iron-containing polysilazane. *Appl. Organomet. Chem.*, **2003**, *17*, 120-126.
[<http://dx.doi.org/10.1002/aoc.400>]
- [35] Li, J.; Zhang, Z.; Zheng, Z.; Guo, L.; Xu, G.; Xie, Z. Preparation and Magnetic Properties of Fe/Si/C/N Ceramics Derived from a Polymer Precursor. *J. Appl. Polym. Sci.*, **2007**, *105*, 1786-1792.
[<http://dx.doi.org/10.1002/app.26161>]
- [36] Mishra, R.; Tiwari, R.K.; Saxena, A.K. Synthesis of Fe-SiC nanowires via precursor route. *J. Inorg. Organomet. Polym.*, **2009**, *19*, 223-227.
[<http://dx.doi.org/10.1007/s10904-009-9259-7>]
- [37] Yan, X.H.; Cheng, X.N.; Han, G.C.; Hauser, R.; Riedel, R. Synthesis and Magnetic Properties of Polymer Derived Metal/SiCN ceramic composites. *Key Eng. Mater.*, **2007**, *353-358*, 1485-1488. 
- [38] Park, J.H.; Park, K.H.; Kim, D.P. Superparamagnetic Si₃N₄-Fe-Containing Ceramics Prepared from a

- Polymer-metal Complex. *J. Ind. Eng. Chem.*, **2007**, *13*, 27-32.
- [39] Yan, X.; Cheng, X.N.; Li, C.S.; Hauser, R.; Riedel, R. Synthesis and Low Temperature Magnetic Properties of Metal Elements Filled Polymer-Derived SiCN Ceramic Composites. *Mater. Sci. Forum*, **2007**, *546-549*, 2269-2272.
[http://dx.doi.org/10.4028/www.scientific.net/MSF.546-549.2269]
- [40] Hauser, R.; Francis, A.; Theismann, R.; Riedel, R. Processing and magnetic properties of metal-containing SiCN ceramic micro- and nano-composites. *J. Mater. Sci.*, **2008**, *43*, 4042-4049.
[http://dx.doi.org/10.1007/s10853-007-2143-3]
- [41] Singh, G.; Priya, S.; Hossu, M.R.; Shah, S.R.; Grover, S.; Koymen, A.R.; Mahajan, R.L. Synthesis, electrical and magnetic characterization of core-shell silicon carbo-nitride coated carbon nanotubes. *Mater. Lett.*, **2009**, *63*, 2435-2438.
[http://dx.doi.org/10.1016/j.matlet.2009.08.025]
- [42] Francis, A.; Ionescu, E.; Fasel, C.; Riedel, R. Crystallization behavior and controlling mechanism of iron-containing Si-C-N ceramics. *Inorg. Chem.*, **2009**, *48*(21), 10078-10083.
[http://dx.doi.org/10.1021/ic900934u] [PMID: 19788256]
- [43] Vakifahmetoglu, C.; Pippel, E.; Woltersdorf, J.; Colombo, P. Growth of one-dimensional nanostructures in porous polymer-derived ceramics by catalyst-assisted pyrolysis. Part I. Iron catalyst. *J. Am. Ceram. Soc.*, **2010**, *93*, 959-968.
[http://dx.doi.org/10.1111/j.1551-2916.2009.03448.x]
- [44] Ionescu, E.; Terzioglu, C.; Linck, C.; Kaspar, J.; Navrotsky, A.; Riedel, R. Thermodynamic control of phase composition and crystallization of metal-modified silicon oxycarbides. *J. Am. Ceram. Soc.*, **2013**, *96*, 1899-1903.
[http://dx.doi.org/10.1111/jace.12327]
- [45] Zhou, C.; Yang, L.; Geng, H.; Zheng, Q.; Min, H.; Yu, Zh.; Xia, H. Preparation of Si-C-N-Fe magnetic ceramic derived from iron-modified polysilazane. *Ceram. Int.*, **2012**, *38*, 6815-6822.
[http://dx.doi.org/10.1016/j.ceramint.2012.05.080]
- [46] Zaheer, M.; Schmalz, T.; Motz, G.; Kempe, R. Polymer derived non-oxide ceramics modified with late transition metals. *Chem. Soc. Rev.*, **2012**, *41*(15), 5102-5116.
[http://dx.doi.org/10.1039/c2cs15326b] [PMID: 22337594]
- [47] Hojamberdiev, M. Prasad, Ravi Mohan; Fasel, C.; Riedel, R.; Ionescu, E. Single-source-precursor synthesis of soft magnetic Fe₃Si- and Fe₅Si₃-containing SiOC ceramic nanocomposites. *Eur. J. Ceram. Soc.*, **2013**, *33*, 2465-2472.
[http://dx.doi.org/10.1016/j.jeurceramsoc.2013.04.005]
- [48] Mera, G.; Gallei, M.; Bernard, S.; Ionescu, E. Ceramic nanocomposites from tailor-made preceramics polymers. *Nanomaterials (Basel)*, **2015**, *5*(2), 468-540.
[http://dx.doi.org/10.3390/nano5020468] [PMID: 28347023]
- [49] Andronenko, S.I.; Stiharu, I.; Menard, D.; Lacroix, C.; Misra, S.K. EPR/FMR, FTIR, X-ray, and Raman investigations of Fe-doped SiCN ceramics. *Appl. Magn. Reson.*, **2010**, *38*, 385-402.
[http://dx.doi.org/10.1007/s00723-010-0120-5]
- [50] Andronenko, S.I. Leo, Alfin; Stiharu, I.; Misra, S.K. EPR/FMR investigation of Mn doped SiCN ceramics. *Appl. Magn. Reson.*, **2010**, *39*, 347-356.
[http://dx.doi.org/10.1007/s00723-010-0163-7]
- [51] Bahloul, D.; Pereira, M.; Gerardin, C. Pyrolysis chemistry of polysilazane precursors to silicon carbonitride Part 1. Thermal degradation of the polymers. *J. Mater. Chem.*, **1997**, *7*, 109-116.
[http://dx.doi.org/10.1039/a603165j]
- [52] Gerardin, C.; Taulelle, F.; Bahloul, D. Pyrolysis chemistry of polysilazane precursors to silicon carbonitride Part 2.- Solid-state NMR of the pyrolytic residues. *J. Mater. Chem.*, **1997**, *7*, 117-126.
[http://dx.doi.org/10.1039/a603181a]

- [53] Mukaida, M.; Hiyama, I.; Tsunoda, T.; Imai, Y. Preparation of Fe-Si thin films by chemical vapor deposition *Proc. of 17th International Conference on Thermoelectrics*, Nagoya, Japan 24-28 May 1998 **1998**, pp. 237-240.
[<http://dx.doi.org/10.1109/ICT.1998.740360>]
- [54] Shimizu, T.; Kumeda, M.; Kiriyama, Y. ESR study on sputtered amorphous Si-C, Si-Ge and Ge-C films. *Solid State Commun.*, **1980**, *37*, 699-703.
[[http://dx.doi.org/10.1016/0038-1098\(81\)91081-4](http://dx.doi.org/10.1016/0038-1098(81)91081-4)]
- [55] Ishii, N.; Kumeda, M.; Shimizu, T. The g-values of defects in amorphous C, Si and Ge. *Jpn. J. Appl. Phys.*, **1981**, *20*, L673-L676.
[<http://dx.doi.org/10.1143/JJAP.20.L673>]
- [56] Dyson, J.F. Electron spin resonance absorption in metals. II. Theory of electron diffusion and the skin effect. *Phys. Rev.*, **1955**, *98*, 349-359.
[<http://dx.doi.org/10.1103/PhysRev.98.349>]
- [57] Misra, S.K. Role of exchange interaction in effecting spin-lattice relaxation: new interactions of data on Cr³⁺ in Cu_{2-x}Cr_{2x}Sn_{2-2x} spinel and dangling bonds in amorphous silicon. *Phys. Rev. B*, **1998**, *58*, 14971-14977.
[<http://dx.doi.org/10.1103/PhysRevB.58.14971>]
- [58] Kliava, J.; Berger, R. Size and shape distribution of magnetic nanoparticles in disordered systems: computer simulations of superparamagnetic resonance spectra. *J. Magn. Magn. Mater.*, **1999**, *205*, 328-342.
[[http://dx.doi.org/10.1016/S0304-8853\(99\)00510-7](http://dx.doi.org/10.1016/S0304-8853(99)00510-7)]
- [59] Sawatzky, E. Magnetic and magneto-optical properties of sputtered Fe₃Si₃ films. *IEEE Trans. Magn.*, **1971**, *7*, 374-376.
[<http://dx.doi.org/10.1109/TMAG.1971.1067099>]
- [60] Hines, W.A.; Menotti, A.H.; Budnick, J.I.; Burch, T.J.; Litrenta, T.; Niculescu, V.; Raj, K. Magnetization studies of binary and ternary alloys based on Fe₃Si. *Phys. Rev. B*, **1976**, *13*, 4060-4069.
[<http://dx.doi.org/10.1103/PhysRevB.13.4060>]
- [61] Altshuler, T.S.; Bresler, M.S.; Goryunov, Yu.V. Ferromagnetic Ordering of Iron Impurities in the Kondo Semiconductor SmB₆. *JETP Lett.*, **2005**, *81*, 475-478.
[<http://dx.doi.org/10.1134/1.1984033>]
- [62] *Statistical Physics*, 4th ed; Landau, L.D.; Lifshitz, E.M. Course of Theoretical Physics. Butterworth-Heinemann: Oxford, **1999**, 5, .
- [63] Patashinskii, A.; Pokrovskii, V. *Fluctuation theory of phase transitions*, 1st ed; Pergamon: Oxford, **1979**.
- [64] Kolel-Veetil, M.K.; Keller, T.M. Organometallic Routes into the Nanorealm of Binary Fe-Si. *Materials (Basel)*, **2010**, *3*, 1049-1088.
[<http://dx.doi.org/10.3390/ma3021049>]
- [65] Yelsukov, E.P.; Maratkanova, A.N.; Lomayeva, S.F.; Konyagin, G.N.; Nemtsova, O.M.; Ul'yanov, A.I.; Chulkina, A.A. Structure, phase composition and magnetic properties of mechanically alloyed and annealing quasibinary Fe(70)Si(x)C(30-x) alloys. *J. Alloys Compd.*, **2006**, *407*, 98-105.
[<http://dx.doi.org/10.1016/j.jallcom.2005.05.035>]
- [66] David, B.; Zboril, R.; Mashlan, M.; Grygar, T.; Dumitrache, F.; Schneeweiss, O. Single ferromagnetic behaviour of nanopowders with Fe₃C. *J. Magn. Magn. Mater.*, **2006**, *304*, e787-e789.
[<http://dx.doi.org/10.1016/j.jmmm.2006.02.224>]
- [67] Sürgers, C.; Potzger, K.; Fischer, G. Magnetism of carbon doped Mn₃Si₃ and Mn₃Ge₃. *J. Chem. Sci.*, **2009**, *121*, 173-176.
[<http://dx.doi.org/10.1007/s12039-009-0019-6>]

- [68] Gopalakrishnan, B.; Sürgers, C.; Montbrun, R.; Singh, A.; Uhlarz, M. v. Löhneysen, H. Electronic transport in magnetically ordered $\text{Mn}_3\text{Si}_3\text{C}_x$ films. *Phys. Rev. B*, **2008**, *77*, 104414. [<http://dx.doi.org/10.1103/PhysRevB.77.104414>]